Lecture Notes in Civil Engineering

Dieu Tien Bui
Hai Thanh Tran
Xuan-Nam Bui *Editors*

Proceedings of the International Conference on Innovations for Sustainable and Responsible Mining

ISRM 2020 - Volume 2

Springer

Building a High-Resolution 3D Geotechnical Model of Hanoi City (Vietnam) for Geohazard Assessment and Sustainable Development

Viet-Ha Nhu(✉)

Hanoi University of Mining and Geology, Hanoi, Vietnam
nhuvietha@humg.edu.vn

Abstract. Geotechnical characteristics in three-dimensional form with the full thickness of each layer are an essential tool for analyzing and visualizing the underground conditions, which are useful for civil engineering projects, geologic hazard assessment, and sustainable development. The objective of this study is to propose and verify a procedure for building a high-resolution 3D geotechnical model in Hanoi city (Vietnam). For this regard, a total of 1,386 borehole logs with attributes of 10,278 soil samples and 16,626 in-situ tests during the last 20 years in the city were collected and processed. These data were interpreted and analyzed in a systematic way to integrate into the 3D model. Then, a high-resolution 3D geotechnical model was constructed and visualized the real geotechnical system with 21 Quaternary geotechnical layers, which integrated the attribute of 19 soil parameters and tectonic activities. It is also feasible as a powerful tool for the reproduction and analysis when it allows extracting spatial distribution of any layer (or point, column) in elevation (or depth, volumetric) and any 2D geotechnical map at different elevation or depth. Finally, the results demonstrated the feasibility of the high-resolution 3D geotechnical model of Hanoi city, which provides valuable information for subsurface and geohazard assessment as well as sustainable development study mitigation.

Keywords: 3D geotechnical model · Urban planning · Urban geohazard · Hanoi · Vietnam

1 Introduction

Geotechnical conditions and properties play an essential role in dealing with the complicated nature of subsurface as urban development and urban geohazard mitigation. Within the last decades, it has been receiving the attention of many researchers through building high-resolution three-dimensional (3D) geotechnical models [1–3]. Within the framework of urban development, geotechnical characterizations of the foundation are essential information for the urban planning and geohazard assessments of cities. Herein, geotechnical parameters are highly necessary to determine underground spaces accurately for constructions, which helps to establish a safe urban extension and sustainable planning [4, 5].

D. Tien Bui et al. (Eds.): *Proceedings of the International Conference on Innovations for Sustainable and Responsible Mining*, LNCE 108, pp. 39–57, 2021.
https://doi.org/10.1007/978-3-030-60269-7_3

Literature review shows that urban geohazards involving ground instability can be costly, dangerous, and affect many people. Some urban geohazards such as land subsidence and liquefaction have become a global problem that many parts of the world have to face. They cause various damages to roads, bridges, buildings, underground infrastructures, and may alter groundwater flows and rivers [6]. For this regard, information on the high-resolution geological-geotechnical maps plays critical roles in geohazard predictions and mitigations.

The geotechnical characterization is typically investigated, stored, and represented in (one-dimensional - 1D) borehole logs, cross-sections, or (two-dimensional - 2D) ground surface maps associating with soil properties. Therefore, several geotechnical characteristics are still not so well estimated in these traditional representations, especially for complicated problems as land subsidence and liquefaction [7–10].

From the development of information technology in recent years, high-resolution 3D geotechnical models have been strengthened research and development. Initially, they were developed as 3D geo-models that mainly used to solve problems in hydrological geology, resource protection, or in the oil and gas industry to simulate and predict the distribution of oil resources, then expanded to serve for other fields such as construction engineering, geotechnics, numerical analysis. Up to now, most of the efforts in the world have focused on the accuracy and reliability improvements of 3D geo-models, including the development of 3D geotechnical models with high-resolution. Many optimization analysis algorithms have been developed and applied over the years. These are essential tools for increasing the quality of modeling of surface structures in underground space. The high-resolution 3D geotechnical models have the potential to apply quite diversified, but the actual number of development models is still limited. The main reason is that they need a large and standardized database. The slow development of data digitization, modeling, and high computerization applications in the field of geosynthetics surveys is a significant obstacle to the cost of modeling [3, 11–13].

The objective of this study is to propose and verify a procedure for production a high-resolution 3D geotechnical model of Hanoi city (Vietnam) using the variogram and kriging interpolation techniques. Then, the model was established using 10,278 soil samples and 16,626 in-situ tests from 1,386 borehole logs in the city during the last 20 years. Finally, discussions are given.

2 Study Area

The study area is the Hanoi city (Fig. 1), which located between longitudes 105°45′E and 105°55′E, and latitudes 20°56′N and 21°06′N. It covers an area of about 161 km^2 that consists of 13 districts comprising urban and suburban areas. The study area is bounded by the Red River in the northeast, and two smaller rivers (the Nhue and Tolich Rivers) border the study area in the west and the south. The altitude ranges from 2.2 m to 12.8 m a.s.l where the high-altitude areas are the dykes along the Red River (Fig. 1). The Red River as the main river which provides water for the study area. Its width varies from 480 m to 1,440 m and its riverbed elevation changes from −5.6 m to −8.3 m a.s.l [14].

Geologically, the Hanoi city is situated in the upper part of the Red River delta, which was formed by the sinking of a former mountain region and was filled by alluvial

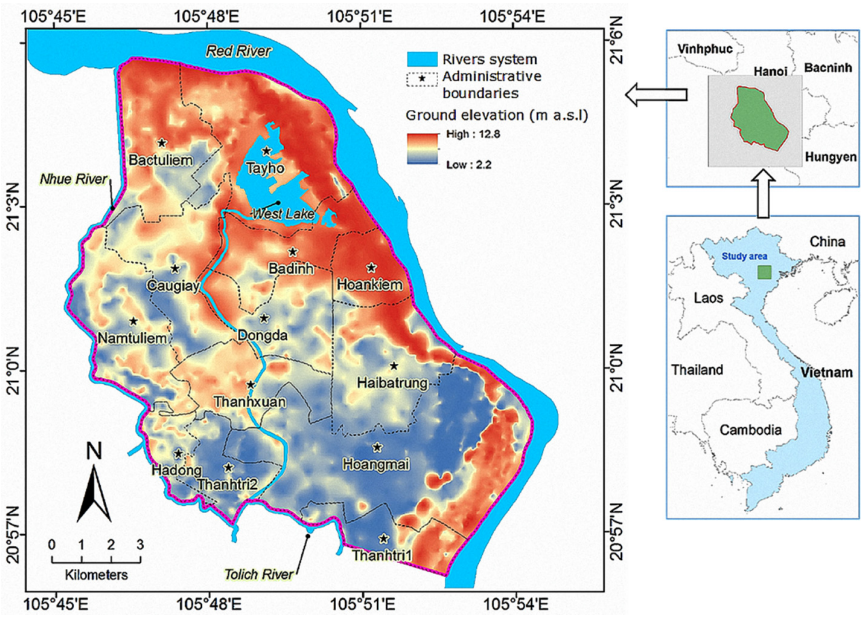

Fig. 1. Location of the study area

deposits of the Red River. The area has undergone periods of active tectonics during the Neogene and the Quaternary. The Neogene sediments are characterized by a thickness of more than 250 m and are mainly composed of sand and gravel. The Quaternary sediments comprise the Pleistocene and the Holocene sediments with a total thickness of about 80–100 m. The Pleistocene sediments consist of gravel, sand, and clay. The upper contact with the Holocene formation is conformable while the lower contact of the formation with Neogene formation is angularly unconformable. The Holocene sediments covering the Hanoi city were deposited as recent alluvium. The composition consists of fine-grained sediments such as sand, silt, and clay, in which there are sporadic occurrences of marine fossils. The formation is a mix of fluvial, lacustrine, and marshy sediments with the dominance of an alluvial origin. On the top are the youngest sediments distributed in the interior side of the Red River dikes and their affluent that are deposited as riverbed-riverbank sediments and anthropogenic embankments. Along the large rivers, it is composed mainly of brownish clayey silt, clay, and sand. While in their affluent, these deposits are yellowish-grey pebble, gravel, and sand mixed with brownish silt and clay (Fig. 1) [15–19].

The Quaternary sediments are a multi-aquifer system consisting of two aquifers of the Holocene and Pleistocene and separated by confining interlayers [20–24]. These consist of six geological formations from old to young: Lechi, Hanoi, Vinh Phuc, Hai Hung, Thai Binh, and anthropogenic deposits. Each geological formation was separated into geological beds in which fining-upward cycles could be recognized in the particle size distribution. A total of 18 geological beds with lithological attributes were delineated in these geological formations (Fig. 2).

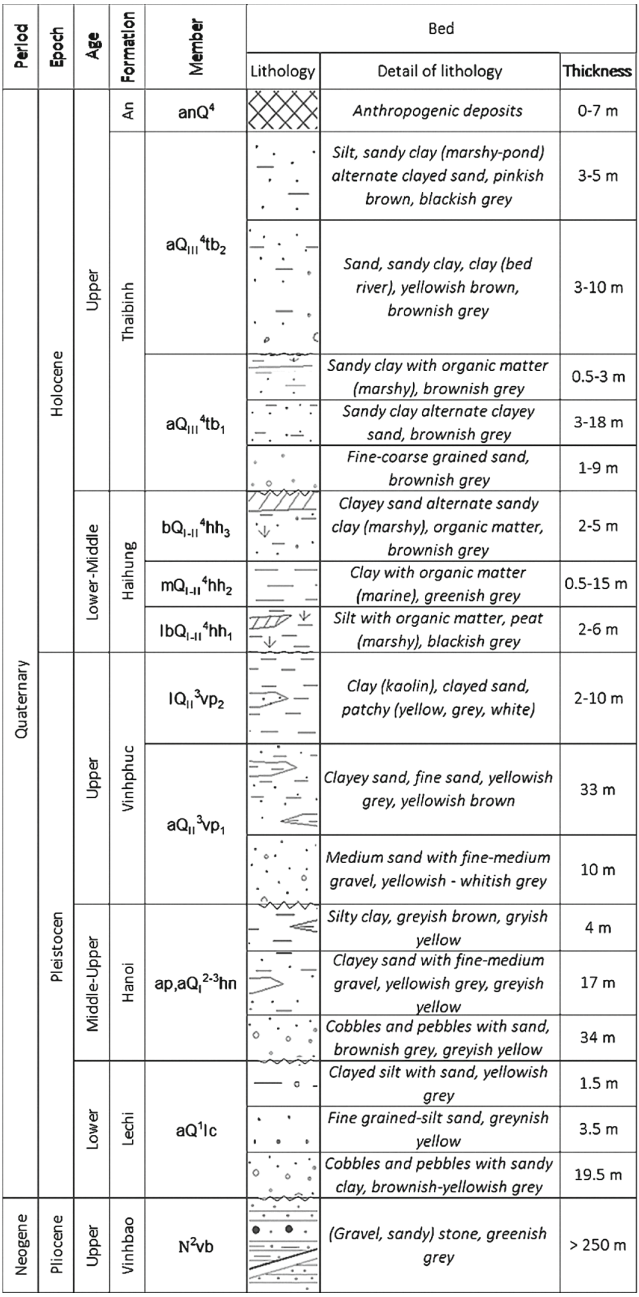

Fig. 2. The lithostratigraphic table of Hanoi city [19]

The faults system in the Hanoi city was mainly tectonically active before the Quaternary but is still having an impact on the Quaternary sediments. Some evidence of faulting

activity has been observed on the ground surface, but interruptions of the deposits are seldom observed in the borehole logs [10, 25]. Based on the geological maps, fault systems were identified comprising the main fault of Vinhninh with the NW-SE trend and the two smaller faults of Nghiado-Tulien and Thanhxuan-Gialam with a NE-SW trend. All of them are normal faults. The Vinhninh fault goes through the center of the Hanoi city and has a length of 18–20 km, displacement of 2–3 km, and a brecciated fault zone of 400–500 m. The fault has been tectonically active since the Paleozoic-Mesozoic and played an important role in the Cenozoic. The Thanhxuan-Gialam fault is more than 15 km long and has a brecciated fault zone of 200–300 m. The Nghia Do-Tu Lien fault is 20–25 km long, has a 600–700 m wide brecciated fault zone, and lies in the north of the Hanoi city (Fig. 6).

The Hanoi area is situated in the monsoonal region, with hot, rainy and dry seasons. During the last decades, the coldest month is January with an average temperature of 16.8 °C, whereas the hottest month is July with an average temperature of 29.3 °C. The maximum evaporation occurs in June with an average value of 99.1 mm, while the minimum occurs in February with an average value of 52.5 mm. The rainy season is generally from May until October and is characterized by high temperatures and humidity. Rainfall in the rainy season occurs with high frequency and intensity and accounts for 80 to 90% of the annual rainfall [26].

3 Data and Materials

Data for high-resolution 3D geotechnical modeling focus on the topographic surface, geological settings, borehole logs, and property attributes [2]. Among them, the most important is probably the borehole logs, which are generally obtained from directly subsurface observation. They supply all information about coordinates, address, starting elevation, down-hole depth, and lithological attributes. The lithological attributes comprise material descriptions and properties from in-situ and laboratory tests. The topographic surface data are the upper limit of the models and are critical for modeling if ground elevations are missing in the borehole logs. The geological settings are essential data to identify sedimentary deposits, geotechnical layers, and tectonic activities.

Based on the availability and knowledge of the Hanoi city, the data was used including (i) national topographic maps at a scale of 1:2,000 [27]; (ii) Hanoi maps of Quaternary sediments, geology, and lithology at a scale of 1:50,000 [16, 19, 28]; (iii) 1,386 borehole logs with attributes of 10,278 soil samples; and (iv) 16,626 in-situ tests. These borehole logs were coming from 348 geotechnical investigation projects during the last 20 years at Hanoi city.

4 Methodology

All available traditional geotechnical collected data was and analyzed in a systematic way by an elaborate data analysis to build a high-resolution 3D geotechnical model off Hanoi city, that included three main components as ground surface, subsurface, and attributes.

For the ground surface, a Digital Elevation Model (DEM) is considered as the most useful for representation. In addition, high-resolution DEMs are always critical to modeling when ground elevations are missing in the borehole logs. Thus, the high-resolution DEM of the 3D geotechnical model was generated from the national topographic maps on the scale of 1:2000 [27]. The raster elevation contours must first be converted to vectors to be "tagged" with their corresponding elevation values. These contour lines were used as input to build a TIN and then rasterized to a DEM, which can be accomplished by GIS tools.

Subsurface models are typically constructed based on a number of measured points obtained from subsurface depths. When the number of measured points is large enough and regularly distributed, high-resolution subsurface models can be constructed by directly connecting the observations [29–31]. If there are few measured points or if they are scattered, realistic subsurface models can only be constructed by interpolation. The subsurface was constructed by spatial analysis supplemented by a cross-validation step for every geotechnical layer (GL). The spatial database was done using Microsoft Excel 365, spatial analysis and interpolation were done using ArcGIS 10.3.

The spatial datasets for subsurface were extracted from measured points as a top elevation of the different GLs in borehole logs. Before that, this data was cleaned, inspected of consistency. Both consistency of the coordinates and the starting elevations of the borehole logs needed to be verified to ensure the quality of data for geospatial analysis. Every GL in every drilling record was then interpreted. A GL was defined as a group of observed lithologies that satisfy stratigraphic conditions [32, 33], including (i) same geological formation or bed, (ii) similar composition, (ii) same compactness, or consistency, and (iv) same stratigraphic order. Considering the stratigraphic conditions, the lithology of borehole logs and the stratigraphy of the Quaternary sediments were matched. Along with each drilling record, every GL thickness was also determined based on its top and base elevation, the top was defined as the base of the layer above. These values were derived from the ground elevation minus the depths of down-holes. Missing GLs between interpreted ones were assigned a zero thickness so that the top and base elevation have the same value. Similarly, all in-situ tests and soil samples within each GL were used to construct spatial datasets of soil properties. They were also used as supplementary information for GL interpretation.

The spatial datasets of every GL are filtered to serve for subsurface interpolations using geostatistical analysis which supplemented by a cross-validation step [34, 35]. The geostatistical analysis used the stochastic and structural spatial variability of natural phenomena and was based on the theory of spatial random variables. The spatial distribution of the attributes of the spatial datasets was to be analyzed by variogram analysis [36, 37]. This interpolation was predicted unknown values based on the statistical relationships among the measured points, including the fitted model from the variography analysis (Fig. 3). Prior to the geostatistical analysis, spatial trends were identified and removed prior to semivariogram analysis, which is performed on the residuals.

For a stochastic variable $V(z)$, if the cumulative distribution of $V(z_i)$ is equal to the cumulative distribution of $V(z_i + b)$, the variable satisfies the strict stationarity hypothesis.

$$F_{z_1,z_2,\ldots\ldots,z_n}(V_1, V_2, \ldots\ldots, V_n) = F_{z_1+b,z_2+b,\ldots\ldots,z_n+b}(V_1, V_2, \ldots\ldots, V_n) \quad (1)$$

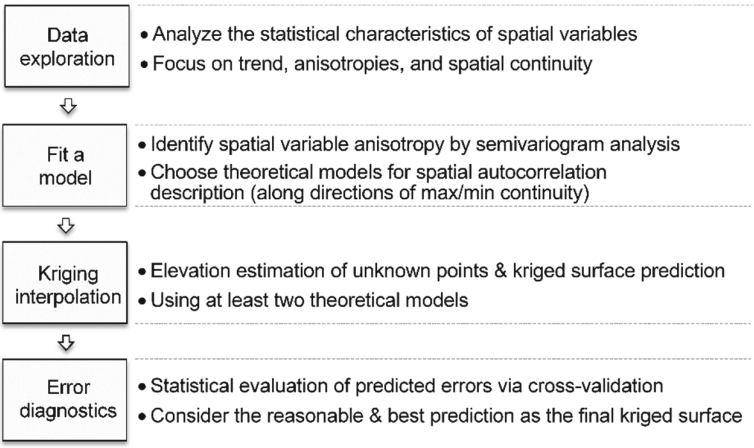

Fig. 3. The flowchart of the geostatistical analysis in this research

where z is the vector of spatial coordinates, V(z) is the variable under consideration as a function of spatial location and b is the lag vector representing a separation between two spatial locations.

The spatial variable normally cannot comply with this very strict stationarity hypothesis. Thus, geostatistics was employed to the estimation of a spatial variable V(z) if the second-order stationarity hypothesis can be satisfied that consists of the following two conditions in the research area:

(1) The mathematical expectation of V(z) exists as a constant as bellowing:

$$E[V(z)] = E[V(z+b)] = m \tag{2}$$

(2) In the research area, the covariance of V(z) exists and depends only on the lag vector b, not on the location z, as belows:

$$\begin{aligned} \mathrm{Cov}\{V(z), V(z+b)\} &= E[V(z)V(z+b)] - E[V(z)]E[V(z+b)] \\ &= E[V(z)V(z+b)] - m^2 = C(b) \end{aligned} \tag{3}$$

$$\text{when } b = 0 \rightarrow \; C(0) = \mathrm{Cov}\{V(z), V(z)\} = \mathrm{Var}[V(z)].$$

where m is a constant value, E[V(z)] is the mathematical expectation of V(z), $\mathrm{Cov}\{V(z), V(z+b)\}$ is the covariance function of V(z) and V(z + b), C(b) is the covariance of distance b, Var[V(z)] is the variance of V(z).

The $\mathrm{Cov}\{V(z), V(z+b)\}$ is assumed to exist in the second-order stationarity hypothesis. In fact, stochastic variables do not have a covariance, but their variogram can be found. Thus, an even weaker stationarity hypothesis called the intrinsic hypothesis can be satisfied if the following two conditions are met as bellowing:

(1) The mathematical expectation $[V(z) - V(z + b)]$ is equal to zero as:

$$E[V(z) - V(z + b)] = 0 \tag{4}$$

(2) The variance of $[V(z) - V(z + b)]$ exists and is stationarity:

$$\mathrm{Var}[V(z) - V(z + b)] = E[V(z) - V(z + b)]^2 \tag{5}$$

Semivariogram analysis is fitting a theoretical model through the experimental semivariogram function (Eq. 6), for whole pairs of locations separated by a distance b as:

$$\begin{aligned}\gamma(b) &= \frac{1}{2}\mathrm{Var}[V(z) - V(z + b)] \\ &= \frac{1}{2}E[V(z) - V(z + b)]^2 - \{E[V(z) - V(z + b)]\}^2\end{aligned} \tag{6}$$

Under the condition of the intrinsic hypothesis, $E[V(z) - V(z + b)] = 0$, the variogram is defined as:

$$\begin{aligned}\gamma(b) &= \frac{1}{2}E[V(z) - V(z + b)]^2 \\ &\approx \frac{1}{2N(b)}\sum_{i=1}^{N(b)}[V(z_i) - V(z_i + b)]^2\end{aligned} \tag{7}$$

where $N(b)$ is the number of data pairs separated by b.

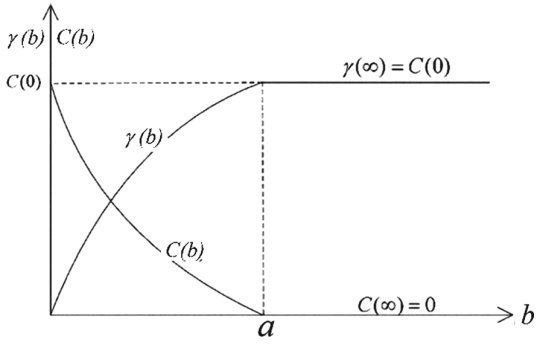

Fig. 4. Relationship between covariance and semivariogram under condition of second-order stationarity

Under the second-order stationarity hypothesis $\gamma(b) = \mathrm{Cov}(0) - \mathrm{Cov}(b)$, which is illustrated in Fig. 4, the semivariance $\gamma(b)$ increases, and covariance $\mathrm{Cov}(b)$ decrease when the distance b increases. However, if b is larger than a value a, both the $\gamma(b)$ and $\mathrm{Cov}(b)$ will level off. The variogram $\gamma(b)$ reaches the maximal value of $\mathrm{Cov}(0)$

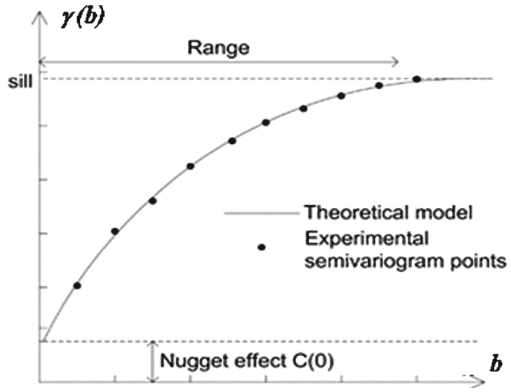

Fig. 5. Experimental semivariogram and fitted theoretical model

and Cov(b) reaches zero. Here the value reflects the autocorrelation influence spectrum, which is called the range of the variogram. At separation distances between zero and the spatial variable is auto-correlated.

The experimental semivariogram is only indirectly used in the geostatistical estimation procedure. It is only used for fitting by theoretical models because the experimental variograms cannot leak the semivariance values at a lag distances continuous series. Therefore, continuous theoretical variogram models are defined, which are described by their range, sill, and nugget (Fig. 5). The total sill (sill + nugget) is value of the semivariance when the semivariogram levels off. It corresponds to the maximum autocorrelation distance among the measured points. The nugget value reflects the variable changing at two very close points, that can sometimes be related to measurement errors or insufficiency of data pairs at the smallest lag distances. The range value as the distance at which the semivariogram value reaches the total sill value, where data pairs are still auto-correlated.

Equations of common theoretical models of the Nugget, Spherical, Exponential, Gaussian, and Power are illustrated in Eq. 8.

$$
\begin{aligned}
&+\text{Nugget:}\quad \gamma(b) = \begin{cases} 0 \text{ if } b = 0 \\ c \text{ otherwise} \end{cases};\\
&+\text{Spherical:}\quad \gamma(b) = \begin{cases} c \cdot \left(1.5\left(\frac{b}{a}\right) - 0.5\left(\frac{b}{a}\right)^3\right) & \text{if } b \le a \\ c & \text{otherwise} \end{cases}\\
&+\text{Exponential:}\quad \gamma(b) = c \cdot \left(1 - \exp\left(\frac{-3b}{a}\right)\right)\\
&+\text{Gaussian:}\quad \gamma(b) = c \cdot \left(1 - \exp\left(\frac{-3b^2}{a^2}\right)\right)\\
&+\text{Power:}\quad \gamma(b) = c \cdot b^w \;\; 0 < w < 2, \;\; c \text{ is the sill value}
\end{aligned}
\tag{8}
$$

Kriging interpolation weights the nearby known values to get a prediction for an unmeasured location (Eq. 9). There are several Kriging interpolation methods. However,

the Ordinary Kriging one is suitable for prediction less trending variable and stationarity hypothesis [38].

$$V(x_0) = \sum_{(i=1)}^{n} \lambda_i \cdot V(x_i) \tag{9}$$

where $V(x_0)$ is the predicted value, λ_i and $V(x_i)$ are measurement and the weight of the nearby location. Minimal variance and no bias of prediction errors are two requirements for λ_i selection as:

$$\begin{aligned} &+ \text{Optimal:} \quad \text{Var}[V(x_i) - V(x_i)] = \min \\ &+ \text{Un - bias:} \quad E[V(x_i) - V(x_i)] = 0 \end{aligned} \tag{10}$$

Cross-validation is performed as a statistical calculation of the predicted error diagnostics that indicate whether the adopted theoretical models are reasonable for prediction [39]. Cross-validation removes one point at a time from the dataset of sample, and then the other ones are used to predict the removed sample via theoretical models. Every sample will have both actual and predicted values for every sample point, and the error is defined as the difference between them when through doing the same procedure piecewise as above.

Finally, the interpolated results then assessed based on statistical evaluation metrics with Correlation Coefficient (R), Mean Error (ME) and Root Mean Square Error (RMSE) as shown in Eq. 11, 12 and 13, respectively. The best-interpolated model will be the one for which R-value is close to one, ME value is close to zero, and RMSE value is minimal. The ME value is near zero when the prediction errors are unbiased. The model result is underestimated if ME value is positive, whereas it is considered to be overestimating if its value is negative [40–44].

$$R = \frac{\sum_{i=1}^{n} (x_i - \overline{x})(y_i - \overline{y})}{\sqrt{\sum_{i=1}^{n} (x_i - \overline{x})^2 \cdot \sum_{i=1}^{n} (y_i - \overline{y})^2}} \tag{11}$$

$$ME = \frac{\sum_{i=1}^{n} (x_i - y_i)}{n} \tag{12}$$

$$RMSE = \sqrt{\frac{\sum_{i=1}^{n} (x_i - y_i)^2}{n}} \tag{13}$$

where $x_1, x_2, \ldots, x_n$ are the predicted values, $y_1, y_2, \ldots, y_n$ are the actual values, $\overline{x}$ and $\overline{y}$ are the mean of predicted and actual values, respectively.

The attributes were considered as additional information about the geotechnical behavior of the different layers, such as soil properties and tectonic activities. The soil

properties comprise the physico-mechanical parameters that are obtained from both laboratory and in-situ tests. The spatial datasets of soil properties, the in-situ tests, and soil samples are analyzed per geotechnical layer. A total of 19 parameters are considered as soil property attributes for each geotechnical layer: The particle size limits of gravel, sand, silt, and clay are >2 mm, 0.06–2 mm, 0.002–0.06 mm, and <0.002 mm, respectively. Consequently, the soil is gravel or sand if it contains more than 50% gravel- or sand-sized particles by mass. On the contrary, the soil is fine-grained if it contains more than 50% silt- and clay-sized particles by mass [45]. The void ratio (e) and porosity (n) are the ratios of the void-space volume to the solids volume and the total volume, respectively. The moisture content or water content (W_n), in percent, is the quantity of water contained in a soil, which is defined as the ratio of the water mass to the solid mass. In the case of fine-grained soils, any change in moisture content results in a change in engineering properties. The liquid limit (WL) is the moisture content at which the changing of soil state from liquid to plastic one.

On the other hand, the moisture content at which the changing of soil from plastic to a semisolid one is defined as the plastic limit (WP). They are generally referred to as the Atterberg limits or consistency limits. The difference between the WL and the WP is defined as the plasticity index (PI). The liquidity index (LI) is the ratio of the difference between the W_n and WP to the PI. Moreover, the compressibility characteristics of fine-grained soils are represented by the coefficients of compressibility (a_V) and the volume compressibility (m_v). Both a_V and m_v are strongly dependent on the pressure level. The a_V is defined as the slope of the void ratio versus the effective stress curve from the oedometer test. The m_v is defined as the ratio of a_V to $(1 + e_i)$ with e_i being the initial void ratio. For coarse-grained soils, the elastic modulus (E) represent for the compressibility characteristic. It is defined as tensile stress - tensile strain ratio. The soil internal friction is defined as the angle on the graph (Mohr's Circle) of the shear stress and normal effective stresses at which shear failure occurs that can be obtained from a triaxial stress test or a direct shear [46]. Besides the mass of size particles, fine-grained soil is defined as an organic or soft soil based on additional physico-mechanical parameters. Soils are defined as very soft if the liquidity index >1, the void ratio >1, the angle of internal friction <100 deg, and the compressibility coefficient >0.1 cm^2kg^1 [10, 45, 47, 48].

Tectonic activities were interpreted based on the fault system. However, these geological properties could not be fully represented in 2D by the strike and dip only. Based on the volumetric body of the high-resolution 3D geotechnical model, the planes of faults could be reconstructed using ArcScene through associating polygonal lines by direct triangulation of digitized faults from the geological map. The dipping direction of faults is simplified by having a constant slope. The volumetric body of the high-resolution 3D geotechnical model is constructed by putting the DEM and all the interpolated top elevations of geotechnical layers in stratigraphic order.

5 Results and Discussion

Since exhaustive geotechnical characterization for 3D modeling, all available traditional geotechnical data was collected and analyzed in a systematic way to integrate into

the model by an elaborate data analysis. The domain of the model was taking into consideration the overall objective and available geotechnical data in the Hanoi city and surroundings. Within this domain, the model had been based on the interpolation of the real geotechnical system. The high-resolution 3D geotechnical model was constructed with three main components, including (i) ground surface, (ii) subsurface, and (iii) attributes.

From the sedimentary conditions and the geotechnical characteristics and available borehole logs, the modeling area was delineated as a rectangular area, including the Hanoi city or area of interest. The domain stretches from longitudes 105°41′E to 105°56′E and from latitudes 20°53′N to 21°07′N, it has an area of about 652 km^2. In the vertical direction, the domain is bounded on top by the ground surface so that it includes the Quaternary sediments. The bottom limit of the domain consists of the Neogene sediment bedrock. Since the Hanoi city is a the Red River delta part, stratification is defined as conformity with continuous sediment deposition (Fig. 1).

The ground surface of the 3D model was constructed as a DEM with 30 × 30 m pixel size. Its altitude ranged from 2.2 to 13.8 m a.s.l and gradually inclines towards the southeast. The highest altitude areas were also present along the main rivers as dykes (Fig. 1).

The subsurface of the 3D model included 21 geotechnical layers that were defined and interpreted. They were assigned from 1 to 21 by descending stratigraphic order and are correlated to the formations of geology. The spatial database for these geotechnical layers was constructed as a database in Microsoft Excel with four separate files (borehole logs, geotechnical layers, in-situ tests, and laboratory test) that related to each other by the key field of "drilling record name". Since the large variety in the depth of the borehole logs, the amount of information from borehole logs decrease with depth. Therefore, for the deep geotechnical layers, less data points with elevation data were available. After trend identification elimination, variograms of the residual datasets of the 20 geotechnical layers were calculated and interpolated by Kriging. The final experimental and modeled variograms for these top surfaces are listed in Table 1 (Figs. 7 and 8).

The values of R, RMSE, and ME of the actual versus the predicted elevations correspond to (0.81–0.94), (-0.001–0.081 m), (0.59–3.92 m) for all 20 geotechnical layers are satisfactory. It should be noted, however, the predicted elevations were slightly underestimated for geotechnical layers 11, 12, & 21 and overestimated for geotechnical layer 20. These errors can probably be attributed to the scattered spatial distribution of drilling record locations and the complexity of the geological system. The prediction error indices from cross-validation and the interpolated elevations of the geotechnical layers are shown in Table 1 and Fig. 6, respectively.

Based on visual inspection of the results, the predicted elevations of all layers are gradually decreasing from the north (mountain region) to the south of the Hanoi city. Geotechnical layer 20 is the thickest with predicted top and base elevations of (−20 m, −48.8 m) and (−50.1 m, −70.8 m). The base surface of this geotechnical layer is also the base surface of the Quaternary sediments or the top surface (geotechnical layer 21) of the Neogene bedrocks. The thinnest geotechnical layers are layer 18 and two groups of layers comprising layers 2 to 7 and layers 10 and 11, respectively.

Table 1. Final theoretical variogram models and the prediction error indices through cross-validation of top elevation values of the geotechnical layers (GL)

GL	Final theoretical model	Sill (m^2)	Nugget (m^2)	Major range (m)	Minor range (m)	Major direction (deg)	Lag (km)	R	RMSE (m)	ME (m)
2	Exponential	4.99	0.06	19.560	29.340	38.1	2.45	0.93	0.69	−0.001
3	Gaussian	0.92	0.12	1.096	924	93.0	0.14	0.92	0.80	−0.005
4	Exponential	4.88	0.13	20.475	30.713	33.2	2.56	0.89	0.80	−0.004
5	Spherical	3.89	0.31	8.587	12.880	31.3	1.07	0.85	0.99	−0.002
6	Gaussian	1.59	0.13	1.610	1.815	175.8	0.20	0.94	0.59	0.005
7	Gaussian	1.49	0.32	1.224	1.016	104.9	0.15	0.90	0.72	0.006
8	Spherical	8.63	1.48	685	916	29.5	0.07	0.83	1.59	0.015
9	Exponential	20.31	0.00	803	1.154	14.6	0.10	0.81	3.92	−0.021
10	Gaussian	16.65	3.07	1.429	1.210	106.9	0.18	0.86	2.30	−0.013
11	Gaussian	19.46	2.99	1.391	1.571	4.4	0.17	0.90	2.40	−0.053
12	Gaussian	24.20	2.95	1.594	1.945	26.4	0.20	0.91	2.80	−0.057
13	Gaussian	26.83	4.66	1.388	1.524	13.2	0.17	0.91	2.80	−0.036
14	Gaussian	25.74	4.61	1.682	2.523	19.9	0.21	0.92	2.77	0.016
15	Exponential	118.46	2.50	21.537	15.710	85.3	2.69	0.91	2.95	−0.010
16	Gaussian	27.24	5.89	1.667	1.422	101.3	0.21	0.91	2.45	−0.027
17	Gaussian	21.77	4.49	1.635	1.305	65.0	0.20	0.89	2.56	0.012
18	Gaussian	19.80	5.63	1.562	1.163	60.5	0.19	0.90	2.52	0.019
19	Gaussian	19.00	4.74	1.534	1.026	60.8	0.19	0.94	1.39	−0.005
20	Spherical	7.20	0.00	1.088	622	51.2	0.91	0.92	2.34	0.081
21	Gaussian	15.06	1.61	3.780	4.111	173.7	0.47	0.91	2.80	−0.057

Except for Neogene bedrock, the attributes of the soil properties were defined from in-situ and laboratory tests performed within each GL. The soil properties are described here for four different types of material, such as gravel, sand, clay, and soft (or organic) soils. The gravel soil is found only in GL20 with a composition consisting of cobbles and pebbles with sand. Its properties range as 8.0 ÷ 13.0 MPa in elastic modulus and 25.9 ÷ 101.3 md^{-1} in hydraulic conductivity of 25.9 ÷ 101.3 md^{-1}. The sandy soils were defined as being composed of fine to coarse sands and are found in GLs of 6, 9, 16, and 17. Their properties as 5 ÷ 27 MPa in modulus and 3.0 ÷ 33.1 md^{-1} in hydraulic conductivity. The clayey soils are found in GLs of 1, 3, 4, 5, 8, 13, 14, 15, 18, and 19 with compositions such as clay, sandy clay and clayey sands. The properties of these soils as 25.5 ÷ 35.6% in moisture content, 30.9 ÷ 44.7 in the liquid limit, 21.6 ÷ 25.2% in the plastic limit, 0.77 ÷ 0.99 in void ratio, 9.5 ÷ 8.2*10^{-4} md^{-1} in hydraulic conductivity, and 1.5 ÷ 100.0*10^{-6} $cmkg^{-1}$ in volume compressibility coefficient. The organic soils,

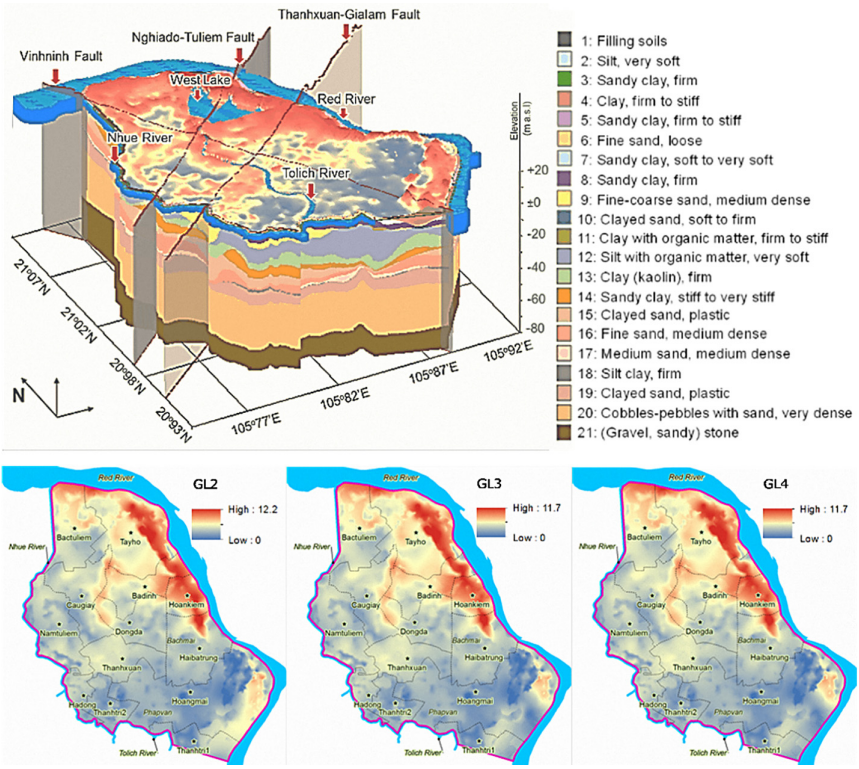

Fig. 6. The high-resolution 3D geotechnical model of Hanoi city with 20 predicted top elevations (m a.s.l) of geotechnical layers and attributions

including silt, mud, peat, and clayey soil, are found in GLs of 2, 8, 11, 12, and 13. Their properties range as 36.3 ÷ 63.7% in moisture content, 42.9 ÷ 62.8% in the liquid limit, 26.8 ÷ 38.2% in the plastic limit, 1.04 ÷ 1.90 in void ratio, and 2.3 ÷ 2.7*10^{-6} $cmkg^{-1}$ in volume compressibility coefficient.

Tectonic activities were interpreted based on the fault system. However, these geological properties could not be adequately represented in 2D by the strike and dip only. Based on the volumetric body of the high-resolution 3D geotechnical model, the planes of faults were reconstructed by direct triangulation through associating polygonal lines of digitized faults from the geological map. The dipping direction of faults is simplified by having a constant slope.

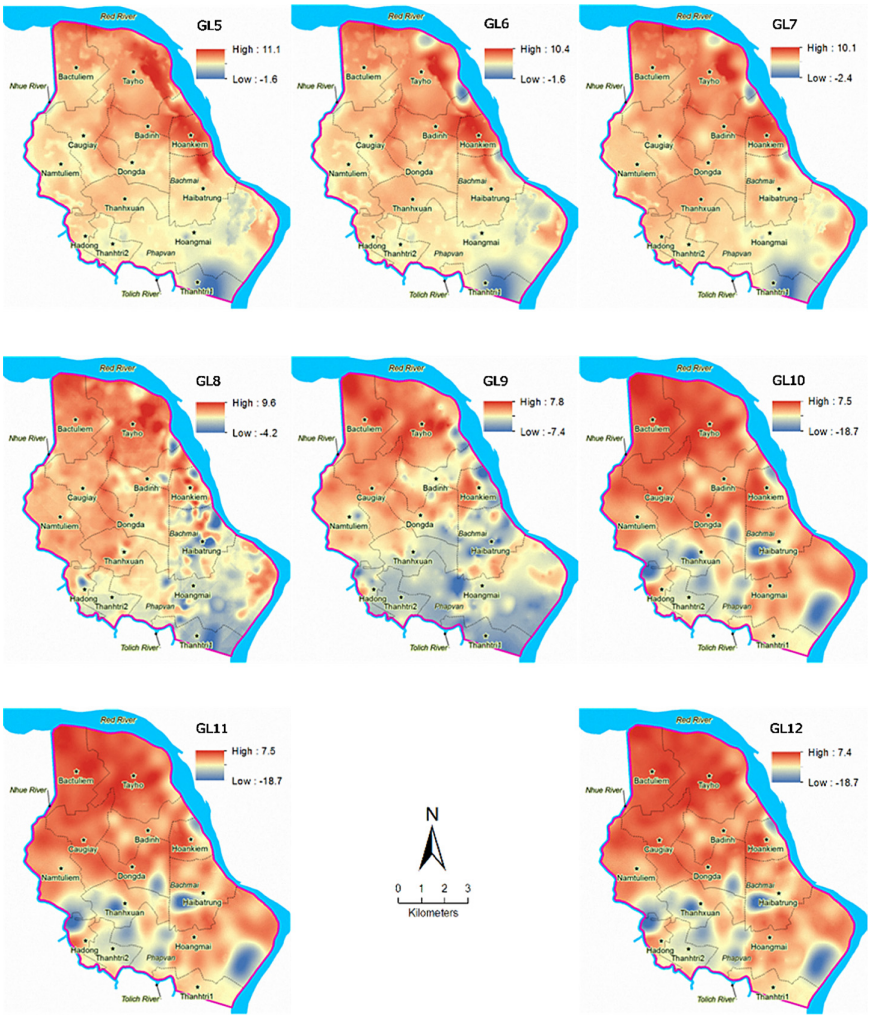

Fig. 7. The high-resolution 3D geotechnical model of Hanoi city with 20 predicted top elevations (m a.s.l) of geotechnical layers and attributions (1st continued)

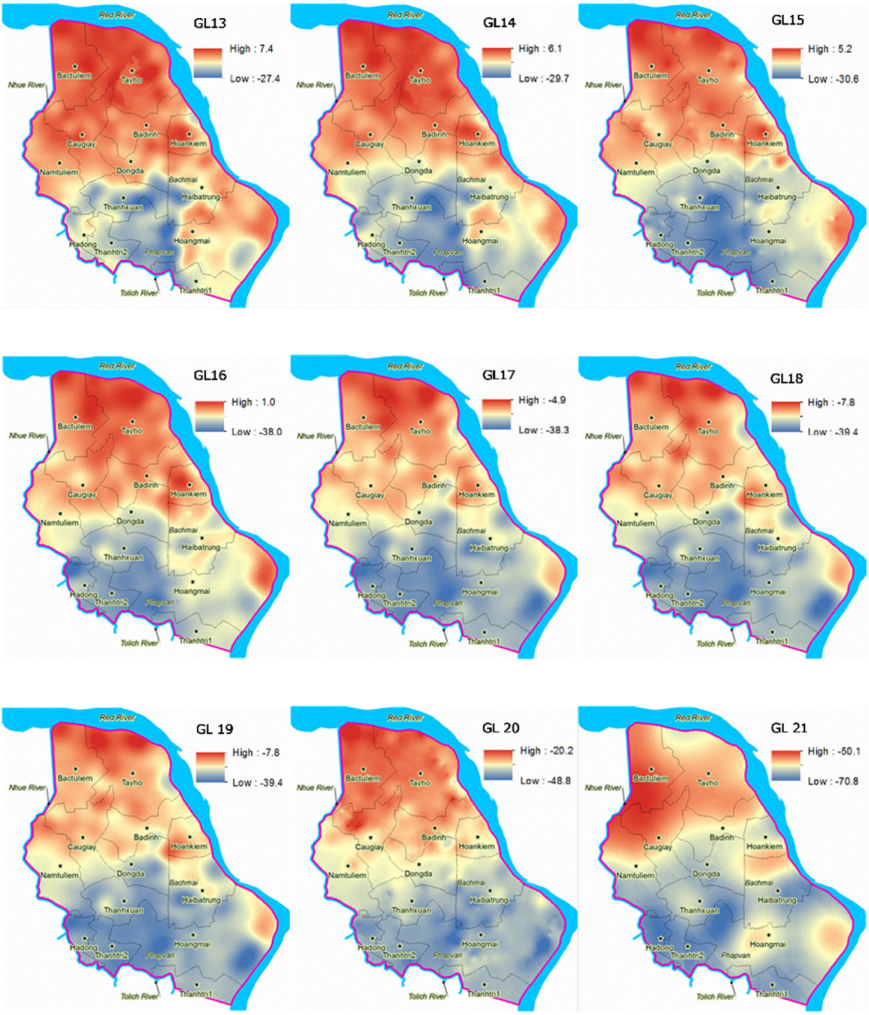

Fig. 8. The high-resolution 3D geotechnical model of Hanoi city with 20 predicted top elevations (m a.s.l) of geotechnical layers and attributions (2nd continued)

6 Conclusion

In this study, a high-resolution 3D geotechnical model of Hanoi city was build using maps (topography, Quaternary sediments, geology), geotechnical data (1,386 borehole logs with attributes of 10,278 soil samples and 16,626 in-situ tests), and geostatistical analysis supplemented by cross-validation. The high-resolution 3D geotechnical model of Hanoi city provided an exhaustive geotechnical characterization with a total of 21 volumetric GLs with the attribute of 19 soil parameters and tectonic activities. The findings of them were satisfactory from statistical evaluation metrics. It is also feasible as a powerful tool for the reproduction and analysis when it allows extracting spatial

distribution of any layer (or point, column) in elevation (or depth, volumetric) and any 2D geotechnical map at different elevation/depth.

From the resultant model, challenges were solved such as (1) the complexity of geotechnical conditions have been transited to a computational representation; (2) the collected and archived data have been increasing quantity, their increased sophistication could be used to improve the variogram analysis results with a better interpolation; (3) the complexity of subsurface was constructed by systematic geostatistical analysis; and (4) the high-resolution 3D geotechnical model could allow performing complex analyses and computations on the geo-framework for different usage.

By this study, it is the first-time geotechnical characterization of Hanoi city was reproduced with high-resolution in comparison with previous studies [7, 8, 10, 21, 49–51].

It is possible that, demonstrated feasibility of the high-resolution 3D geotechnical model of Hanoi city using the proposed methodology. From it, valuable information could be provided for dealing with the complicated environment of subsurface as urban development and geohazard mitigation for the Hanoi city.

Acknowledgments. The author would like to thank Prof. Marijke Huysmans from VUB-HYDR, who provide the language and help.

References

1. Azaronak, N.: Building 3D models from geotechnical data (2015)
2. Dong, M., Neukum, C., Hu, H., Azzam, R.: Real 3D geotechnical modeling in engineering geology: a case study from the inner city of Aachen. Germany. Bull. Eng. Geol. Environ. **74**(2), 281–300 (2015)
3. Lelliott, M., Bridge, D.M., Kessler, H., Price, S., Seymour, K.: The application of 3D geological modelling to aquifer recharge assessments in an urban environment. Q. J. Eng. Geol. Hydrogeol. **39**, 293–302 (2006)
4. El May, M., Dlala, M., Chenini, I.: Urban geological mapping: geotechnical data analysis for rational development planning. Eng. Geol. **116**, 129–138 (2010)
5. Haeri, S.: The role of geotechnical engineering in sustainable and resilient cities. Sci. Iran. **23**, 1658–1674 (2016)
6. Galloway, D., Burbey, T.: Review: regional land subsidence accompanying groundwater extraction. Hydrogeol. J. **19**, 1459–1486 (2011)
7. Dai, N.D.: Report on the results of the Hanoi Urban Geological Survey. Federation II - GeoHydrology, Department of Geology of Vietnam, Hanoi (1996)
8. Federation II - GeoHydrology: Report on Geological Investigation of Hanoi - Hai Phong - Quang Ninh Economic Corridor. Federation II - GeoHydrology, Department of Geology of Vietnam, Hanoi (1996)
9. Thang, L.T.: Studying the types of soft ground structures in Hanoi area and assessing their ability to use them in construction. vol. Ph.D. Hanoi University of Mining and Geology (1995)
10. Phuong, N.H., Thinh, T.D., Ty, P.V., Tuong, D.T., Hong, N., Tinh, N.V., Vu, T.X., Hai, H.V., Bat, D.V., Long, N.H., Quang, N.H., Phong, N.V., Phuc, D.D., Binh, T.T., Tuan, P.M., Huong, P.T., Minh, P.V., Nga, P.T.V., Long, N.T., Nu, N.T., Hung, N.V., Hai, P.H., Hung, N.M., Thong, V.D.: Collection and verify data for supplement studying of soft soil zonation mapping in Hanoi area (TC-ĐT/06-02-03) (2004)

11. Robins, N., Davies, J., Dumpleton, S.: Groundwater flow in the South Wales coalfield: historical data informing 3D modelling. Q. J. Eng. Geol. Hydrogeol. **41**, 477–486 (2008)
12. Roy, D., Robinson, K.E.: Surface settlements at a soft soil site due to bedrock dewatering. Eng. Geol. **107**, 109–117 (2009)
13. Lelliott, M., Cave, M., Wealthall, G.: A structured approach to the measurement of uncertainty in 3D geological models. Q. J. Eng. Geol. Hydrogeol. **42**, 95–105 (2009)
14. CWRCT: Report of geodesy investigation of Red River at scale of 1:5000. Center for Water Resources Consultant and Technology Transfer (CWRCT) (2010)
15. Tanabe, S., Saito, Y., Lan Vu, Q., Hanebuth, T.J., Lan Ngo, Q., Kitamura, A.: Holocene evolution of the Song Hong (Red River) delta system, northern Vietnam. Sediment. Geol. **187**, 29–61 (2006)
16. VIGMR: Hanoi geological map at scale of 1:50000. Vietnam Institute of Geosciences and Mineral Resources (VIGMR) (2010)
17. Mathers, S., Zalasiewicz, J.: Holocene sedimentary architecture of the Red River delta, Vietnam. J. Coast. Res. **15**, 314–325 (1999)
18. Funabiki, A., Haruyama, S., Van Quy, N., Van Hai, P., Thai, D.H.: Holocene delta plain development in the Song Hong (Red River) delta, Vietnam. J. Asian Earth Sci. **30**, 518–529 (2007)
19. VIGMR: Hanoi quaternary deposit map at scale of 1:150,000. Vietnam Institute of Geosciences and Mineral Resources (VIGMR) (1995)
20. Nguyen, D.D.: Report on investigation of urban geology for Hanoi city. Department of Hydrogeology 2 (1996)
21. Thu, T.M., Fredlund, D.G.: Modelling subsidence in the Hanoi City area, Vietnam. Can. Geotech. J. **37**, 621–637 (2000)
22. Giao, P.H., Ovaskainen, E.: Preliminary assessment of Hanoi land subsidence with reference to groundwater development. Lowl. Technol. Int. **2**, 17–29 (2000)
23. VIGMR: Hanoi hydrological map at scale of 1:50000. Vietnam Institute of Geosciences and Mineral Resources (VIGMR) (2010)
24. Jusseret, S., Tam, V.T., Dassargues, A.: Groundwater flow modelling in the central zone of Hanoi, Vietnam. Hydrogeol. J. **17**, 915–934 (2009)
25. Hai, H.V.: Some new discovery about new tectonic in Hanoi area and surroundings. J. Geol. A, 42–49 (2007)
26. NHMS: Report of metorological data in range of 1980–2013 at Hanoi hydro-metorological station. National hydro-metorological service (2014)
27. NARENCA: Topographic maps at scale of 1:2000. Viet Nam Publishing House of Natural Resources, Environment and Cartography (NARENCA) (2000)
28. VIGMR: Hanoi lithological map at scale of 1:50000. Vietnam Institute of Geosciences and Mineral Resources (VIGMR) (2010)
29. Pollard, D.D., Fletcher, R.C.: Fundamentals of Structural Geology. Cambridge University Press, Cambridge (2005)
30. Delaunay, B.: Sur la sphere vide. Bull. Acad. Sci. USSR **7**, 793–800 (1934)
31. Peucker, T.K., Fowler, R.J., Little, J.J., Mark, D.M.: The triangulated irregular network. In: American Society of Photogrammetry. Proceedings of the Digital Terrain Models Symposium, p. 532
32. Bondarik, G.K.: Dinamitreckoe i xtatitreckoe zondirovanie gruntop Vinginemoi geolopi. M. Nedra (1964)
33. RockWare: RockWorks15 Manual. RockWare, Inc. (2008)
34. Matheron, G.: Principles of geostatistics. Econ. Geol. **58**, 1246–1266 (1963)
35. Krige, D.G.: A statistical approach to some basic mine valuation problems on the Witwatersrand. J. Chem. Metall. Min. Soc. South Afr., 201–223 (1951)

36. Webster, R.: Quantitative spatial analysis of soil in the field. Adv. Soil Sci. **3**, 1–70 (1985)
37. Isaaks, E.H., Srivastava, R.M.: An introduction to applied geostatistics. AMC **10**, 12 (1989)
38. Pyrcz, M.J., Deutsch, C.V.: Geostatistical Reservoir Modeling. OUP USA (2014)
39. Erdogan, S.: A comparision of interpolation methods for producing digital elevation models at the field scale. Earth Surf. Proc. Land. **34**, 366 (2009)
40. Schlumberger: Visual Modflow user's manual. Waterloo Hydrogeologic, Waterloo, ON (2010)
41. Feng, S., Huo, Z., Kang, S., Tang, Z., Wang, F.: Groundwater simulation using a numerical model under different water resources management scenarios in an arid region of China. Environ. Earth Sci. **62**, 961–971 (2011)
42. Schoups, G., Addams, C.L., Gorelick, S.: Multi-objective calibration of a surface water-groundwater flow model in an irrigated agricultural region: Yaqui Valley, Sonora, Mexico. Hydrol. Earth Syst. Sci. Discuss. Discuss. **2**, 2061–2109 (2005)
43. Witten, I.H., Frank, E.: Data Mining: Practical Machine Learning Tools and Techniques, 2nd Edition. Morgan Kaufmann, Burlington, 2005 (2011)
44. Ormsby, T., Napoleon, E., Burke, R., Groessl, C., Bowden, L.: Getting to Know ArcGIS Desktop. Esri Press Redlands, Redlands (2010)
45. TCVN: Vietnamese standards for soil classification 5747:1993, vol. 5747:1993, p. 10 (1993)
46. Smoltczyk, U.: Geotechnical Engineering Handbook. Ernst & Sohn, Berlin (2003)
47. TCXD: Ground Improvement by Prefabricated Vertical Drain (PVD), vol. 245-2000, p. 10 (2000)
48. 22TCN: Instruction of investigation and design automobil embankment on soft soil foundation, vol. 262–2000, p. 51 (2000)
49. Manh, N.D., Lan, N.N.: Geo-environment with efficient exploitation and use of Hanoi urban underground space (2010)
50. Yonezawa, G.: Developing of 3D urban modeling of Hanoi. Intriguing ASIA **113**, 168–174 (2008)
51. Yonezawa, G.: 3D topographical analysis of Hanoi, Vietnam. Southeast Asian Stud. **46**, 519–531 (2009)